ELSEVIER

Contents lists available at ScienceDirect

Extreme Mechanics Letters

journal homepage: www.elsevier.com/locate/eml



A designer's challenge: Unraveling the architected structure of deep sea sponges for lattice mechanical metamaterials



Zacharias Vangelatos ^a, M. Erden Yildizdag ^{b,c}, Costas P. Grigoropoulos ^{a,*}

- ^a Department of Mechanical Engineering, University of California, Berkeley, CA, 94720, USA
- ^b Faculty of Naval Architecture and Ocean Engineering, Istanbul Technical University, Istanbul, 34469, Turkey
- c International Research Center for the Mathematics and Mechanics of Complex Systems (MeMoCS), University of L'Aquila, L'Aquila, 67100, Italy

ARTICLE INFO

Article history: Received 24 December 2022 Received in revised form 11 March 2023 Accepted 27 March 2023 Available online 29 March 2023

Keywords: Hierarchical mechanical behavior Bioinspired design In situ SEM microindentation Atomic force microscopy FEA modeling

ABSTRACT

Biomimetic and Bioinspired designs have been investigated due to the advances in modeling, mechanics and experimental characterization of structural features of living organisms. To accomplish bioinspiration for fields such as robotics, adhesives and smart materials, it is required to comprehend how Nature accomplished enhanced mechanical behavior. Among the plethora of complex organisms spanning at different lengthscales, the deep sea sponge Euplectella Aspergillum has been of particular interest due to its lattice structure that can be the framework to design mechanical metamaterials. However, despite its intriguing morphology, constraints in the fabrication and modeling of scalable and nonuniform materials has hindered the study of its mechanical performance and how to harness it. Moreover, a comprehensive FEA model that encompasses the whole spectrum of its constitutive and structural performance has not been reported. In this study, it is aimed to characterize and model the mechanical behavior of this sponge from a structural standpoint. Utilizing various experimental techniques, an FEA mechanical model is developed to study the nonlinear buckling analysis of the sponge's lattice structure and its resilience to failure. Finally, through topology optimization and sensitivity analysis, a new mechanical metamaterial is proposed. Our results elucidate how mechanical characterization and FEA modeling can be employed for a deeper understanding of Nature's tailored hierarchy and the design of metamaterials.

© 2023 Elsevier Ltd. All rights reserved.

1. Introduction

The advances in the modeling of coupled phenomena such as thermal-fluid, mechanics, mechanical behavior of materials and optics, combined with sophisticated characterization techniques for each respective discipline have resulted in an inexorable progress in the structural characterization of living organisms. Nature, possessing millions of years of experience, has realized complex multiscale and hierarchical features which can provide remarkably enhanced performance at various lengthscales. Characteristic examples such as the flower beetle Torvnorrhina flammea possesses a photonic multilayer comprised by micropillars that enhances the mechanical robustness and optical damage tolerance [1]. In addition, the leaf-cutter ant Acromyrmex echinatior [2] possesses a multilayered high-magnesium calcite armor that provides enhanced mechanical behavior. The baleen of the whale Balaena mysticetus [3] has structural features resembling a sophisticated composite material with extremely high resilience to fracture. The fur of the bear Ursus maritimus [4] is comprised of a "smart textile", which provides optimal thermal insulation. In addition, the diabolical ironclad beetle Phloeodes diabolicus [5] has adaptive "hinges" and structural defects that enable high strength and resistance to failure under incredibly high loads. The Amazon river fish Arapaima gigas [6] has multilayered fish scales, resembling a 3D composite structure, which significantly enhances the fracture toughness and resilience to crack propagation of the fish. The Japanese jewel beetle Chrysochroa fulgidissima [7] also possesses a multilayered structure comprised of photonic crystals at different orientations, resulting in angledependant reflection. Finally, the explosive pygidial defensive system of bombardier beetles such as the Brachinus, Pheropsophus and Aptinus has a funnel-shaped structure with honeycomb geometry, enabling contraction and large deformations to evade damage during the explosive discharge [8]. Furthermore, fluid mechanics simulations and turbulence experiments have been employed to study the effect of the scale's morphology on the hydrodynamic perfomance of different shark species, such as the Isurus oxyrinchus, Carcharhinus Galapagensis, Sphyrna zygena and Carcharhinus obscurus [9]. Specifically, these micrometer features can be modeled as small plate element that have a significant impact on the drag and shear stress imposed at the surface of the shark.

^{*} Corresponding author.

E-mail address: cgrigoro@berkeley.edu (C.P. Grigoropoulos).

For the efficient characterization of all these remarkable instances, techniques such as nanoindentation, reflectance spectroscopy, x-ray powder diffraction (XRD), energy-dispersive x-ray spectroscopy (EDS), scanning electron microscopy (SEM), transmission electron microscopy (TEM) and thermal imaging were combined with FEA simulations to unravel the optical, thermal and mechanical properties as specific lengthscales.

Biomimetic methodologies have led to the design of novel nanocomposite materials, such as a tailored seashell structure for enhanced ultrastrong materials that could be employed for space vessels [10]. Since all of these extraordinary properties are the ramification of their hierarchical and microscale structure, the recent progress in microscale additive manufacturing techniques has paved the way to imitate such features and patterns. Specifically, techniques such as one-photon and multiphoton lithography have provided complex 3D structures resembling natural constructs with extremely high resolution, spanning from a few hundreds of nm to mm [11,12]. Consequently, these techniques have resulted in photonic crystals and antireflective surfaces inspired by the structure of the moth Plutella xylostella [13-15]. Furthermore, these techniques can also provide significantly more complex patterns using self-assembly processes. Of particular interest are fiber structures, such as silk fibroins and spider silks, which are well known for their exceptional mechanical properties, and have a great potential to be utilized for engineering materials. These fibers are protein based, formed through self-assembly and have been widely employed for regenerative and reparative medicine [16]. Self-assembled biomolecular nanostructures [17] are particularly attractive, due to their biocompatibility and amenability to rational modification. Robust techniques for self-assembling biomolecular structures have been developed and shown the integration of these materials on MPL structures, realizing a scaffold-on-scaffold fabrication process [18, 19] for nonuniform materials. To incorporate complex structural features with nm resolution into the architected material, we have employed the guided self-assembly of block copolymers (BCPs), a "bottom-up" self-assembly that offers a wide variety of periodic nanostructures, such as lamellae, spheres, cylinders, or gyroids, with feature sizes of 5 to 200 nm. These fabrication techniques have resulted in the realization of nanoscale spiral features, which would potentially be employed as energy dissipation and fracture impedance mechanisms through controlled contact and densification [20]. This principle has been elucidated in nanolabyrinth ultra thin structures, sustaining large reversible deformations [21].

These techniques and methods have also accentuated the study of metamaterials. Metamaterials, structures possessing properties bestowed by their architected structure rather than their bulk material, have also been thoroughly fabricated and tested [22]. Thus, complex 3D structures possessing controlled buckling mechanisms [23,24], high resilience to fracture [25] and tailored nonlinear deformations [26,27] have been designed, fabricated and tested. Typically these structures are comprised of lattice members, which can be easily realized by lithography techniques. These lattice structures can possess intricate designs, such as architected defects for controlled deformation mechanisms [28,29], which can be either organized or randomly distributed for the case of irregular metamaterials [30]. In addition, they can furnish whelked features for enhanced strength through friction [31] and plate lattice elements for optimal stiffness and isotropy [32].

In particular, architected defects and nonuniformities is a successful design approach observed in nature to improve the directional strength of an organism or create hybrid structures comprised of different materials [33–35]. These strategies are primarily focused on the increase of the fracture toughness and

the fracture impedance through distribution of different materials or voids to isolate the crack front.

A bridge between the domain of bioinspired structures and that of mechanical metamaterials can be found at the bottom of the sea, on the intriguing world of deep sea sponges. Deep sea sponges possess a skeleton that consists of spicules made from amorphous hydrated silica bonded by additional silica layers [36]. Furthermore, they encompass calcite reinforced silica to silica joints, which lead to extraordinary strong cross-spicule linkages [37,38]. It has been observed that these layers form concentric tubes with optimal relative thickness for maximized strength [39]. An intriguing finding is that these features can also be found in much larger spicules, such as those of Monorhaphis chuni [40,41]. Consequently, they also provide an exceptional design for crack propagation impedance and enhanced fracture toughness, and also remarkable enhanced hardness and stiffness compared to bulk silica or other CaP, CaCO₃ and CaF based organisms such as the bone, sea shells and urchins respectively [36,42]. It has been proposed that these features are derived by biosintering mechanisms of biosilica nano-hybrid particles within and among siliceous spicules [43]. Nevertheless, among the plethora of different deep sea sponges, one that has captured the attention of researchers is Euplectella aspergillum [39,44–46]. The structure of this sponge embosoms a spiral hierarchical design with members of different thickness and angle of orientation at specific distances, forming a unique structural pattern. This structure has been geometrically modeled and has inspired the design of mechanical metamaterials [47] due to its remarkable resilience to buckling. Moreover, its unique shape has also been elucidated from the perspective of fluid mechanics to explain how it affects the flow field and the internal vortical structure, facilitating the selective filter feeding of the organism [48].

Despite all of these results, there are still some questions associated with the modeling of Euplectella aspergillum. Specifically, the different structure of the various lattice members insinuates different mechanical behavior and nonuniform constitutive response. In addition, the effect of this nonhomogeneous behavior across different lattice members and the structural stability of the sponge needs to be addressed. Answering these questions would provide a systematic way to model, simulate and design bioinspired designs for enhanced structural stability. This study aims to address the above topics by merging in-situ nanomechanical testing, high resolution Helium Ion Microscopy (HIM) imaging. FEA modeling, optimization and sensitivity analysis for the study of the mechanical response of these sponges. By extracting the constitutive behavior of the material, an FEA model is realized to conduct nonlinear buckling analysis on the structure. Finally, through topology optimization and sensitivity analysis, an optimum design is provided with respect to the buckling behavior of the structure to design a new mechanical metamaterial. These results show how experiments and FEA can be merged to explain the mechanical behavior of natural systems and lead to improved structures for the design of novel mechanical metamaterials.

2. Mechanical characterization of deep sea Sponge's skeletal structure

2.1. XRD and EDX characterization

To study the mechanical performance of the sponges, 5 samples obtained by Tarpon Springs, Florida were utilized. To validate their chemical composition and microstructure, XRD characterization was conducted using the Panalytical X'Pert Pro. In addition, EDS was employed using the Hitachi 2460 with KEVEX which is inserted at the SEM FEI Quanta 3D FEG. For the XRD analysis, spicules from the different samples were prepared by hand grinding using a mortar and pestle to conduct powder diffraction. For

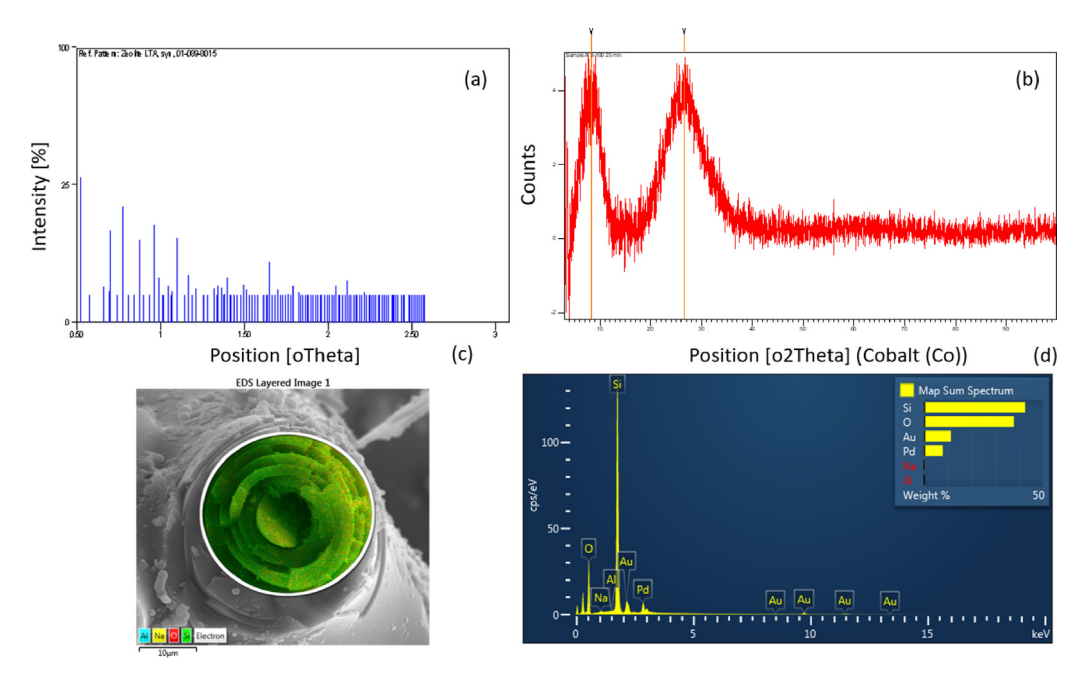


Fig. 1. XRD and EDX characterization of the sponge samples. (a) The stick pattern as it was derived from the X'Celerator fast detector (b) The spectrum of XRD detector. Both the stick pattern and the spectrum are used by the database of the XRD software to find the mineral that would match this pattern and spectrum (c) 3D mapping of the chemical composition of a spicul cross section, showing how the vast majority of the structure is comprised by Si, since Zeolite LTA has high silica composition. (d) The EDX spectrum of the cross section, revealing the chemical components present in Zeolite LTA and proving the correct matching of the XRD database.

the EDS characterization, the SEM beam was focused on cut cross sections of the spicules to conduct 3D EDS mapping. The results are presented in Fig. 1. The x-ray patterns of Fig. 1(a-b) that were compared with the database of known phases using analytical software revealed that the spicules are comprised of Zeolite LTA. It must be noted that the larger range of the peaks shown in Fig. 1(b) should also be attributed to the organic components that these samples have due to the natural environment. To validate the pattern found by the database, the chemical composition derived by the EDS was juxtaposed. The 3D mapping of the cross section and its respective spectrum, shown in Fig. 1(c-d), revealed all the chemical components present in Zeolite LTA, namely Si, O, Na and Al. The presence of Au and Pd is attributed to the sputtering of the samples for high quality imaging and the EDX source. In addition, this form of Zeolite has a high percentage of silica (Si/Al \sim 17) as it shown by the percentages of the spectrum in Fig. 1(d). These results show the same Silica structure that has been reported in previous studies for hardness measurements on spicules of glassy sponges [39,46,49]. Therefore, the samples are representative to derive the constitute equation of each structural layer and characterize their morphology, as it will be presented in the next sections.

2.2. SEM and HIM imaging characterization

To comprehend the different structural layers of the sponge's structure, it was required to delineate the different structural layers and geometric patterns found on its geometry. To accomplish this, the larger features were imaged through the SEM and the much more complex features that required high contrast and resolution through the Helium Ion Microscope (HIM). HIM can provide much high depth of focus compared to the SEM and also does not require sputtering of the samples, which might distort features in the range of few μ m. While several studies have identified the structural characteristics of these samples [45,46], microscale imaging was required to obtain characteristic geometric lengths that will be used in the CAD modeling and also

decipher which structural components must possess different constitutive behavior. Characteristic magnified sections of the structure are shown in Fig. 2. As it is shown in Fig. 2(a) the structure of the sponge has some distinct geometrical features. It is comprised by a cylindrical core, which is covered by a whelked helix (Fig. 2(b)), defined in the literature as the external spiraling ridge [45]. In addition, the circumference of the cylindrical body is comprised of vertical, horizontal, and diagonal struts (Fig. 2(c)), defined as the internal ridge. However, some of these struts have multiple beam members which are multilayered, as shown in Figs. 2(d-f). Studies have focused on the extraordinary strength and resilience to fracture that is caused by this multilayered nature of the individual lattice members (or spicules) [39, 41,46,49]. Apart from higher fracture toughness, they also enhance the stiffness of the nodes since these are regions of higher stress concentration. It has been examined how the thickness of each layer has been optimized to carry the maximum load capacity [39]. However, the number of merged spicules on each different geometrical feature also has a key role in the mechanical performance, since it affects the slenderness of the individual members and their flexural strength. The helix (Fig. 2(b)) has multiple spicules interconnected with each other, and each one of them is multilayered (Fig. 2(f)), having a significant effect in the stiffness of the structure. The horizontal and vertical struts are also comprized by a smaller number of interconnected spicules (Fig. 2(c)). However, as it is also reported elsewhere [45], the diagonal ones are comprised by single spicules. This characterization will guide the mechanical measurements that will be presented in the next section.

2.3. In-situ nanoindentation testing

To unravel the mechanical performance of the different lattice members of the sponge, in-situ nanoindentation tests were conducted using the PI 87 SEM PicoIndenter, Hysitron. The indenter was mounted on the SEM FEI Quanta 3D FEG. To conduct the mechanical test, a molybdenum flat tip (model 72SC-D3/035)

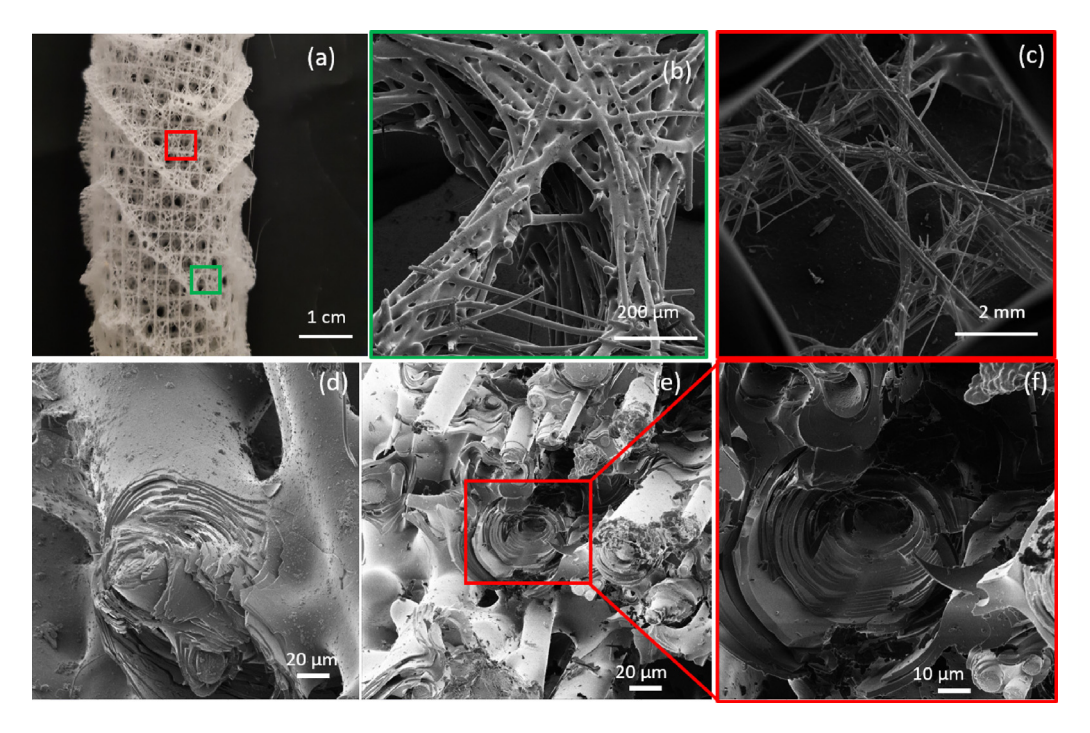


Fig. 2. Mechanical response of different substructures of the sponge. (a) The core of the sponge, revealing distinct geometrical patterns, namely the external ridge and vertical, horizontal and diagonal struts (b) SEM imaging on the external ridge, showing multiple spicules intertwined with each other. (c) SEM magnification on the horizontal, vertical and diagonal struts, showing how the vertical and horizontal are also comprized multiple spicules, while the diagonal are single. (d) HIM imaging on the cross section of a node between the spicules, showing the multiple structure of each member. (e) Cross section cut of the ridge, revealing multiple spicules firmly bonded with each other. (f) Magnified section of (e), showing multiple layers in a representative spicule in the array.

(407A-M) Probing Solutions, Inc.), possessing a 70 µm diameter was utilized. The various spicules were fixed on one side onto an SEM pin stub mount (TED PELLA) 16604-9 or 16111 using a PELCO® Pro C100 Cyanoacrylate Glue (TED PELLA). To improve the imaging, the samples the gold sputtered for 50s using the Magnetron Sputtering Deposition System. While this testing could provide high precision measurements for the mechanical response of conglomerated spicules located at internal and external ridge of the sponge, the mechanical testing of individual fibers observed in the tilted arrays shown in Fig. 3 were too flexible for precise measurement, leading to high noise in the data. To surpass this challenge the individual fibers were mechanically tested using the Atomic Force Microscope Vistascope AFM system from Molecular Vista and the TL-CONT Tipless Contact Mode AFM Cantilever from Nanosensors. The mechanical response for each substructure along with in-situ imaging from the instrument are shown in Fig. 3. The external ridge (Fig. 3(a)) was fixed on both ends to conduct three point bending measurement on the effective length that is bent, while the internal ridge was also fixed in one location for cantilever bending testing (Fig. 3(b)). Video recordings of the mechanical testing are provided in the Supplementary Data (Video A and Video B respectively). The single spicule was fixed on the same sample holder on one side for cantilever measurement as well (Fig. 3(c)), but pressed on both sides for higher rigidity. Representative curves of the results are shown in Fig. 3(d-e) (Video A for 3(d) and Video B for 3(e)). The displacement was normalized to scale the curves and render them easier to be compared. It is shown that external ridge has significantly higher stiffness compared to the internal one. Calculating the stiffness by the deflection equation reveals that its 104.3 \pm 3.8 GPa and 85.1 \pm 4.3 GPa respectively, a result which is consistent with experimental results reported for single spicules [42,46]. It is also noted that since the spicules are firmly bonded with each other (Fig. 2(b)), the behavior is linearly elastic. However, focusing on the AFM measurement of the single spicule (Fig. 3(e)), reveals that during bending the spicule has a nonlinear behavior, which is attributed to the stiffening of the internal layers as they contact each other during bending. These results can be used to define the constitutive behavior of the different geometrical features and create the FEA model that will be discussed in the next section.

3. Finite element analysis

To characterize the mechanical behavior of the lattice structure, finite element analysis simulations were conducted. A finite element model was first generated in a commercial FEA software parametrically. An optimum set of geometric parameters were identified via a topology optimization framework based on linear buckling simulations. Then, a nonlinear buckling analysis and sensitivity analysis were conducted.

3.1. Design and finite element modeling

The sponge's skeleton was first idealized considering the vertical, horizontal and diagonal spicule bundles as the ones that were characterized in the previous section. In our FEA framework, we modeled the sponge as a cylindrical lattice structure, of length L and diameter D, comprised of four main structural elements: straight beams in longitudinal and circumferential directions (internal ridge and single spicules), helical beams of the same dimensions as the previous ones, and a primary semi-elliptical helical beam (external ridge) (see Fig. 4).

We modeled spicule bundles as beam elements; vertical, circumferential and helical beams and the primary helical beam with their respective geometrical features (see Fig. 4(a–c)). The geometric parameters and their initial design values are listed in Table 1. The parameters N_V , N_C , and N_L are the total number of vertical beams, total number of circumferential beams, and number of loops of primary helical beam, respectively. The other parameters, B, H, and R_P , are illustrated in Fig. 4(c–d). The model

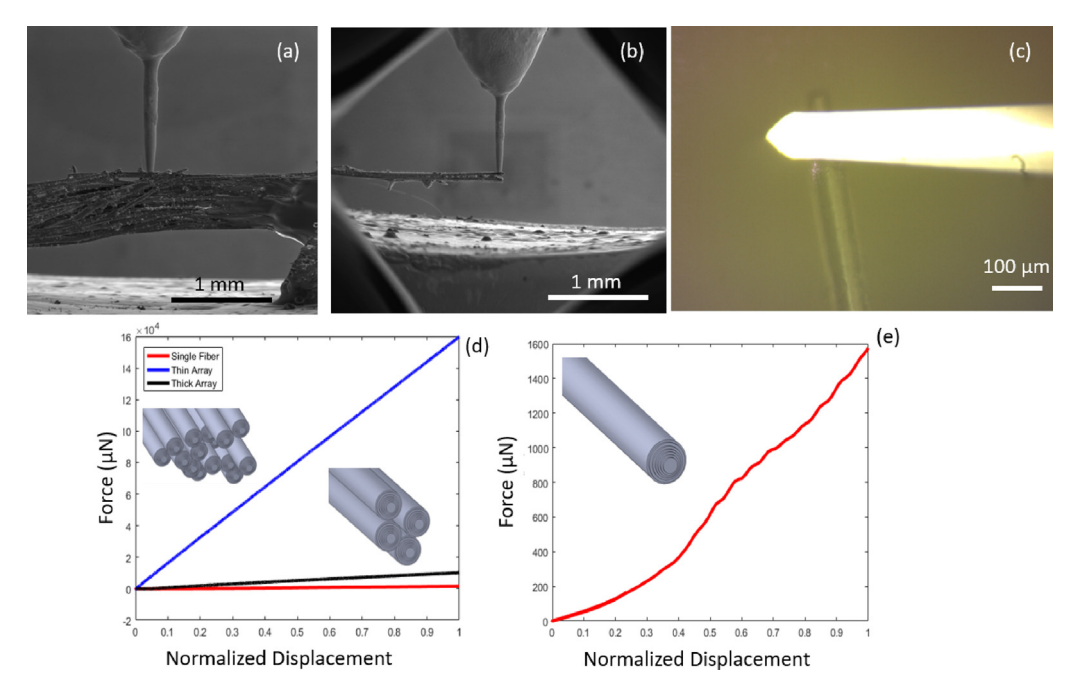


Fig. 3. Mechanical response of different substructures of the sponge. (a) Front view of the micro-indentation bending measurement on the external ridge in the SEM chamber, placing the tip on the straight length of the structure for a uniform cross section. (b) Front view of the micro-indentation bending measurement on the internal ridge in the SEM chamber. (c) Top view from the objective lens of the AFM system of the single spicule for the bending measurement. (d) Representative force–Displacement curves for the three different measurements. The displacement is normalized to scale the curves for easier comparison. (e) Force–displacement curve of the single spicule as it is extracted from the AFM system, revealing a nonlinear behavior associated with the inherent stiffening of the layers as the structure bends.

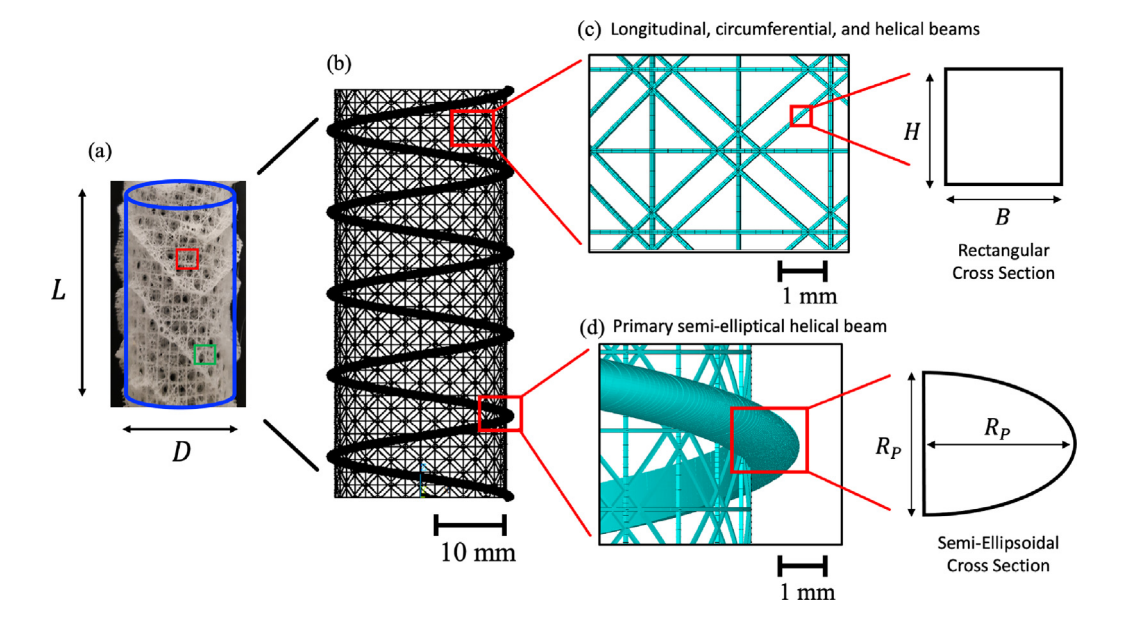


Fig. 4. Finite element model of sponge by using beam elements. (a) Sponge's skeleton. (b) FEA model of the designed cylindrical lattice. (c) Rectangular cross sectional area of longitudinal, vertical, and helical beams (width B and height H). (d) Semi-elliptical cross sectional area of the primary helical beam (radius R_P).

and its mesh were formed in ANSYS[®] Mechanical™ parametrically (with the parameters listed in Table 1) by a developed code written in ANSYS Parametric Design Language (APDL). Hence, different topologies can be easily conceived by changing geometric parameters in the code. The initial FEA model consists of 69285 beam elements (209 604 degrees of freedom) which corresponds to total volume of 2176.3 mm³. While the original sponge possesses multiple semi-elliptical helixes, the metamaterial design was simplified to possess only one to mitigate the computational cost. As it will be shown in the next section, a single helix

will still be sufficient to dictate the mechanical performance of the structure. In addition, since future work would investigate the manufacturability of this geometry, this would simplify the manufacturing process. The other beam elements (Fig. 4(a) and (c)) are the same as the sponge. For the geometrical cross section of Fig. 4(c), a rectangular cross section was selected since the SEM captions (Fig. 2(c)) were stacked in a rectangular pattern rather than circular.

As we consider a sponge living in a deep sea environment, the lattice structure was assumed to be subjected to both axial and

Table 1Initial and optimum values for the geometric parameters.

Parameter	Description	Initial value	Opt. value
L	Length of cylindrical lattice	60 mm	_
D	Diameter of cylindrical lattice	25.2 mm	_
В	Width of cross section	$0.18 \pm 0.1 \; \text{mm}$	0.24 mm
Н	Height of cross section	$0.18 \pm 0.1 \; \text{mm}$	0.24 mm
R_P	Radius of semi-ellipsoidal cross section	$1.2 \pm 0.6 \text{ mm}$	0.8 mm
N_V	Number of vertical beams	36 ± 12	30
N_{C}	Number of circumferential beams	33 ± 12	39
N_L	Number of loops of primary helical beam	5 ± 4	5

circumferential compressive loads while one of its ends is cantilever. The linear buckling analysis was first conducted with the initial design values and the critical buckling load was identified as 134.88 N.

3.2. Topology optimization and sensitivity analysis

To identify optimum set of geometric parameters, the developed APDL code was coupled with Response Surface Optimization module provided in ANSYS[®] DesignXplorer™. A surface response was generated by using the results of 400 numerical simulations. The length and the radius of the cylindrical lattice were kept fixed, and the simulations were conducted by varying other geometric parameters in a specified range (see Table 1). In the optimization framework, we adapted the following objective seeking to maximize the critical buckling load while minimizing the total volume with respect to the volume of the initial design:

$$Objective = \begin{cases} \text{minimize } V(B, H, R_P, N_V, N_C, N_L), & \text{subject to } V \leq V_{init}, \\ \text{maximize } F_{cr}(B, H, R_P, N_V, N_C, N_L). \end{cases}$$

Here, V is the total volume of the structure, F_{cr} is the critical buckling load, and V_{init} is the total volume of the initial design. With the optimum geometric parameters listed in Table 1, the critical buckling load was increased by 280% (378.67 N) while total volume of the structures was decreased by 31.68% with respect to the initial design.

To provide more insight into the mechanical behavior of the lattice structure, a nonlinear buckling analysis and a sensitivity analysis were conducted. The nonlinear buckling analysis was conducted with the determined optimum geometric parameters by introducing an imperfection to the initial geometry. The geometric imperfection was defined by a mode shape obtained by linear buckling analysis. For the numerical solution, the arclength method was utilized with a tolerance of 0.5% for L-2norm of force to control convergence. In sensitivity analysis, the effects of width (W) and height (H) of rectangular cross section, number of loops of primary helical beam (N_L) , and radius of semi-elliptical cross section (R_P) were investigated by computing the critical buckling load. In Fig. 5, the predicted results are presented. Fig. 5(a) shows the deformed shape obtained in the nonlinear buckling analysis at the bifurcation point. Fig. 5(b) presents the critical buckling loads obtained by linear buckling analyses considering longitudinal, circumferential, and both longitudinal and circumferential compressive pressure. The force-displacement obtained regarding to the average longitudinal displacement on the top surface of the lattice structure is given Fig. 5(c). The conducted sensitivity analysis regarding geometric parameters N_I , R_P , W, and H is presented in Figs. 5(d)-(e) and (g-h), respectively. Since the material is brittle, the maximum principle stress is calculated and plotted as a function of the applied force in Fig. 5(f).

4. Results and discussion

The validation of the experimental, FEA and optimization results need to be evaluated under the framework of structural stability and material properties. Through XRD and EDS measurements the authenticity of the specimens was verified. Their composition is that of Zeolite LTA, a material comprised of high silica concentration that bolsters the strength of the nodes in the lattice [38]. This brittle material provides high strength and stiffness that is necessary for such a large and slender lattice structure to remain elastically stable. Therefore, the beam members of the geometry possess high stiffness, as it was shown by the experimental measurements (Fig. 3(d-e)). However, individual structural members possess different material properties due to the different number of spicules. Structures like that can be realized by additive manufacturing using multiple materials [50] or by creating truss structures with different materials [51]. Consequently, this leads to a very stiff primary helical beam that, as it is shown in Fig. 5(a) (subjected to longitudinal and circumferential compressive pressures), dictates the resilience to collapse. The structure deforms under a shell buckling mechanism, where large deformations are observed throughout the whole surface of the geometry. The optimization results show how the improvement is driven by the circumferential buckling, since the longitudinal buckling has the biggest contribution in the critical buckling load and does not vary significantly as a function of the geometrical parameters. To put this into perspective, the longitudinal buckling is two orders of magnitude larger compared to the circumferential buckling (Fig. 5(b)). In addition, the bonding of the multiple ridges and the glassy nature of the sponge material can make it sustain very high stresses in compression as resulted in Fig. 5(f), which shows how the stress evolves with respect to the applied force. As in glassy materials used in engineering applications, the failure occurs at lower stress due to defects and flaws. The optimization resulted in 280% increase in the critical buckling load and 31.68% decrease in the material volume, creating a lighter and more resilient metamaterial design inspired by the sponge's structure. However, it must be noted that the optimized geometrical parameters are not exorbitantly different compared to the sponge's average parameters. The primary helix drives the critical buckling load and its increase dominates the mechanical performance. Nevertheless, the other geometrical parameters are within the range of the measured dimensions. This result would potentially be associated with the fact that the sponge has been evolved in a multi-objective optimization framework, including the drag coefficient [48] for instance. While this study focuses on the design and optimization of mechanical properties, future research should also focus on multi-objective optimization and relevant design constraints to explore different features of the structure and how they can be synergistically utilized to create novel metamaterials and different values that the design variables converge. In addition, it must be pointed out that different material parameters would vary the optimized design parameters. However, as it was observed in previous studies of mechanical metamaterials [24], the geometrical configuration of the beam

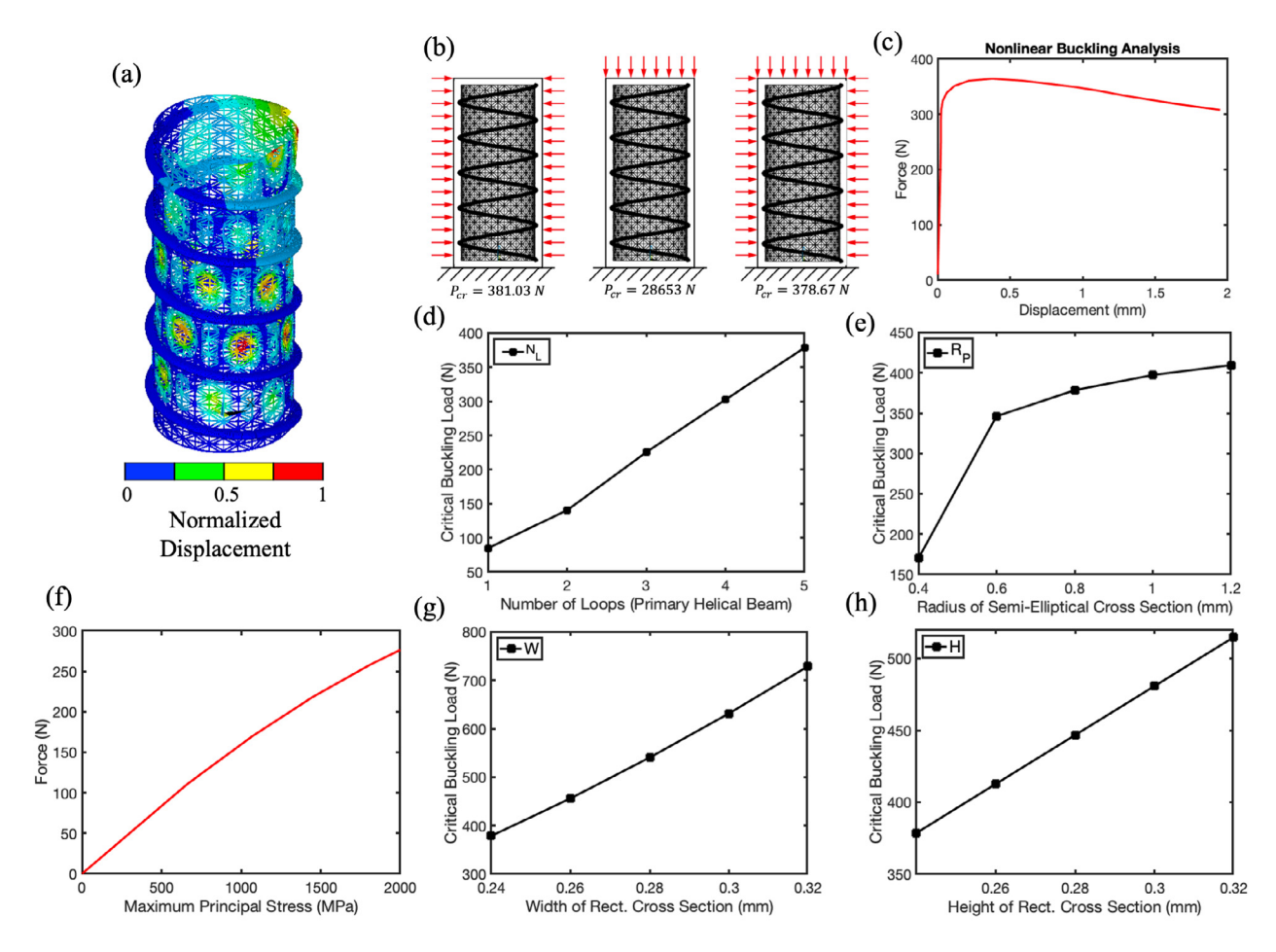


Fig. 5. Nonlinear buckling and sensitivity analyses with the determined optimum geometric parameters. (a) Deformed shape obtained around bifurcation in the nonlinear buckling analysis. (b) Critical buckling loads considering longitudinal, circumferential, and both longitudinal and circumferential compressive pressures s(linear buckling analysis). (c) Force–Displacement curve obtained in the nonlinear buckling analysis. (d)-(e) Sensitivity analysis regarding geometric parameters N_L , R_P , respectively. (f) The reaction force as a function of the maximum principal stress (g-h) sensitivity analysis regarding geometric parameters W, and W respectively.

members dominates the resulting buckling modes. Therefore, the optimum would significantly vary only in the case that a different geometry is utilized. The force displacement curve shown in Fig. 5(c) shows that the instability mechanism of the sponge is bifurcation, leading to nonlinear behavior and negative stiffness due to buckling. This macroscopically lead to shell buckling, as it is shown if Fig. 5(a).

Another result that has a major significance in the design of the metamaterial structure is the effect of the geometrical parameters of the primary helical beam to the critical buckling load. As it is observed in Figs. 5(d-e, g-h), increasing the dimensions of the primary helix, leads to an increase in the critical buckling load. However, regarding the radius of the semielliptical cross section (Fig. 5(e)), the slope of the curve shifts and stabilizes, indicating that creating a thicker cross-section will not have a significant improvement in the mechanical performance. This result is counter-intuitive, since in classical beam theory, decreasing the slenderness of a beam structure will increase the critical buckling load at a constant rate. This behavior should be attributed to the total geometry of the sponge and how all of the parts are assembled to create a single structure. Since there are other arrays such as the internal ridge that are attached to the primary helix, increasing the radius will make these members overlap with each other, negating their effect on the critical buckling load. This result is indicative of the nonlinear behavior of the metamaterial as a function of the geometrical parameters and highlights the importance of optimization to explore how different parameters affect the mechanical performance.

While this study sets the framework to comprehend the structural design of Euplectella Aspergillum with respect to the mechanical performance, it also paves the way for novel metamaterial designs for controlled buckling behavior. Previous studies on lattice structures have focused on the arrangement of straight beam members [24,28,29,52]. However, the present study shows how curved beam members can also be modeled and employed for the design of resilient metamaterials. In addition, future work should also focus on more efficient strategies to model the nonlinear behavior of the helical beams. Methodologies such us higher gradient models [53] can provide analytical expressions for the behavior of the beams and easier finite elements modeling. Moreover, from a structural standpoint, this study investigated the elastic behavior of the structure since brittle materials will fracture and collapse after the elastic regime at the emergence of buckling. While the pre-buckling behavior is crucial for a functional metamaterial, the bonding of the various beam members in the ridges leads to exceptional resilience to fracture. Future work should focus on efficient models to study the crack propagation on the ridges, the effect of scale effects and flaw distributions and create more complex explicit models that incorporate fracture and the complete post buckling regime. This investigation would also lead to novel metamaterials with controlled fracture toughness. Moreover, the different constitutive behavior of the various beam members shows how additive manufacturing with nonuniform materials can be employed to design enhanced architected materials that cannot be realized with uniform material properties [54]. Finally, such designs can be employed for ultra-light,

ultra-stiff materials as in former studies of microscale structures [22]. However, they can also be utilized for the design of stents [55], where the maximization of circumferential and longitudinal buckling is desired for high endurance. Since the mechanical performance is independent of the scale, ultralight sponge-inspired designs can also be used for compliant towers or offshore structure that require high resilience to anchoring strength at high depths. In addition, such designs can also be employed for environments that have high pressure and consequently the designed structures require high resilience to collapse. Characteristic examples are deep sea monitoring robots [56], mems devices that require enhanced rigidity [57,58] and curved beams for higher fracture resistance [59,60].

5. Conclusions

In this study, we characterized the mechanical performance and design of the deep sea sponge Euplectella Aspergillum and used it as a design framework to create a new metamaterial design. Through material characterization and imaging, the mechanical properties and structural configuration was delineated and it was used to create an FEA model for the proposed design. The new metamaterial possesses non-uniform constitute behavior across different beam members, high resilience to buckling and features that are tangible to the ones of the real sponge. This highlights how Nature has optimized the organism with respect to the mechanical performance. Through topology optimization. the metamaterial structure has 280% higher buckling load and 31.68% less volume compared to the original one that uses the dimensions extracted from the Sponge. Our results highlight how mechanical and materials characterization, FEA and optimization can be combined to obtain a better understanding in Nature's hierarchical designs and create novel metamaterials.

CRediT authorship contribution statement

Zacharias Vangelatos: Conceptualization, Data curation, Formal analysis, Investigation, Methodology, Validation, Visualization, Writing – original draft, Writing – review & editing. M. Erden Yildizdag: Data curation, Formal analysis, Investigation, Methodology, Validation, Software, Visualization, Writing – original draft, Writing – review & editing. Costas P. Grigoropoulos: Funding acquisition, Project administration, Resources, Review & editing.

Declaration of competing interest

The authors declare that they have no known competing financial interests or personal relationships that could have appeared to influence the work reported in this paper.

Data availability

Data will be made available on request.

Acknowledgments

This research was partially supported by the National Science Foundation (NSF), USA under the Future Manufacturing Seed Grant Program, Grant No. 2134534. The authors thank Professor P. Hosemann, Department of Nuclear Engineering, University of California, Berkeley, for the availability of his indentation apparatus. The authors thank John L. Grimsich, Manager, Thin Section, SEM, XRD Labs, Department of Earth and Planetary Sciences University of California, Berkeley for assisting in the training of the XRD. The authors thank Dr. F. Allen, Department of Materials Science and

Engineering (UCB) for training to use the helium ion microscope. The nanoindentation, SEM, EDS and HIM experiments were conducted at the California Institute of Quantitative Bioscience (QB3 Lab). The authors also thank Yoonsoo Rho, Laser Thermal Lab, for assisting in the AFM measurements.

Appendix A. Supplementary data

Supplementary material related to this article can be found online at https://doi.org/10.1016/j.eml.2023.102013. The developed ANSYS Mechanical APDL code is available on

https://github.com/yildizdag/sponge.

Video A: Mechanical testing of the external ridge (Magnification 100x, Voltage = 10 kV, Beam Current = 1.75 nA)

Video B: Mechanical testing of the internal ridge (Magnification 100x, Voltage = 10 kV, Beam Current = 1.75 nA)

References

- [1] Z. Jia, M.C. Fernandes, Z. Deng, T. Yang, Q. Zhang, A. Lethbridge, J. Yin, J.-H. Lee, L. Han, J.C. Weaver, et al., Microstructural design for mechanical-optical multifunctionality in the exoskeleton of the flower beetle torynorrhina flammea, Proc. Natl. Acad. Sci. 118 (25) (2021).
- [2] H. Li, C.-Y. Sun, Y. Fang, C.M. Carlson, H. Xu, A. Ješovnik, J. Sosa-Calvo, R. Zarnowski, H.A. Bechtel, J.H. Fournelle, et al., Biomineral armor in leaf-cutter ants, Nature Commun. 11 (1) (2020) 1–11.
- [3] B. Wang, T.N. Sullivan, A. Pissarenko, A. Zaheri, H.D. Espinosa, M.A. Meyers, Lessons from the ocean: whale baleen fracture resistance, Adv. Mater. 31 (3) (2019) 1804574.
- [4] Y. Cui, H. Gong, Y. Wang, D. Li, H. Bai, A thermally insulating textile inspired by polar bear hair, Adv. Mater. 30 (14) (2018) 1706807.
- [5] J. Rivera, M.S. Hosseini, D. Restrepo, S. Murata, D. Vasile, D.Y. Parkinson, H.S. Barnard, A. Arakaki, P. Zavattieri, D. Kisailus, Toughening mechanisms of the elytra of the diabolical ironclad beetle, Nature 586 (7830) (2020) 543–548.
- [6] W. Yang, V.R. Sherman, B. Gludovatz, M. Mackey, E.A. Zimmermann, E.H. Chang, E. Schaible, Z. Qin, M.J. Buehler, R.O. Ritchie, et al., Protective role of Arapaima gigas fish scales: structure and mechanical behavior, Acta Biomater. 10 (8) (2014) 3599–3614.
- [7] F. Schenk, B.D. Wilts, D.G. Stavenga, The Japanese jewel beetle: a painter's challenge, Bioinspiration Biomim. 8 (4) (2013) 045002.
- [8] A. Di Giulio, M. Muzzi, R. Romani, Functional anatomy of the explosive defensive system of bombardier beetles (Coleoptera, Carabidae, Brachininae), Arthropod Struct. Dev. 44 (5) (2015) 468–490.
- [9] B. Dean, B. Bhushan, Shark-skin surfaces for fluid-drag reduction in turbulent flow: a review, Phil. Trans. R. Soc. A 368 (1929) (2010) 4775–4806.
- [10] G. Xu, H. Fan, C.A. McCoy, M.M. Mills, J. Schwarz, Bioinspired synthesis of thermally stable and mechanically strong nanocomposite coatings, MRS Adv. (2022) 1–5.
- [11] A. Marino, C. Filippeschi, V. Mattoli, B. Mazzolai, G. Ciofani, Biomimicry at the nanoscale: current research and perspectives of two-photon polymerization, Nanoscale 7 (7) (2015) 2841–2850.
- [12] L. Jonušauskas, D. Gailevičius, S. Rekštytė, T. Baldacchini, S. Juodkazis, M. Malinauskas, Mesoscale laser 3D printing, Opt. Express 27 (11) (2019) 15205–15221.
- [13] Y.-C. Kim, Y.R. Do, Nanohole-templated organic light-emitting diodes fabricated using laser-interfering lithography: moth-eye lighting, Opt. Express 13 (5) (2005) 1598–1603.
- [14] L.W. Chan, D.E. Morse, M.J. Gordon, Moth eye-inspired anti-reflective surfaces for improved IR optical systems & visible LEDs fabricated with colloidal lithography and etching, Bioinspiration Biomim. 13 (4) (2018) 041001
- [15] M.J. Haslinger, A.R. Moharana, M. Mühlberger, Antireflective moth-eye structures on curved surfaces fabricated by nanoimprint lithography, in: 35th European Mask and Lithography Conference (EMLC 2019), Vol. 11177, International Society for Optics and Photonics, 2019, p. 111770K.
- [16] J.P. Jung, J.Z. Gasiorowski, J.H. Collier, Fibrillar peptide gels in biotechnology and biomedicine, Pept. Sci.: Orig. Res. Biomol. 94 (1) (2010) 49–59.
- [17] H. Long, W. Zeng, H. Wang, M. Qian, Y. Liang, Z. Wang, Self-assembled biomolecular 1D nanostructures for aqueous sodium-ion battery, Adv. Sci. 5 (3) (2018) 1700634.
- [18] V. Dinca, E. Kasotakis, J. Catherine, A. Mourka, A. Ranella, A. Ovsianikov, B.N. Chichkov, M. Farsari, A. Mitraki, C. Fotakis, Directed three-dimensional patterning of self-assembled peptide fibrils, Nano Lett. 8 (2) (2008) 538–543.

- [19] K. Terzaki, E. Kalloudi, E. Mossou, E.P. Mitchell, V.T. Forsyth, E. Rosseeva, P. Simon, M. Vamvakaki, M. Chatzinikolaidou, A. Mitraki, et al., Mineralized self-assembled peptides on 3D laser-made scaffolds: a new route toward 'scaffold on scaffold'hard tissue engineering, Biofabrication 5 (4) (2013) 045002
- [20] J. Choi, S. Koo, I. Sakellari, H. Kim, Z. Su, K.R. Carter, M. Farsari, C.P. Grigoropoulos, T.P. Russell, Guided assembly of block copolymers in three-dimensional woodpile scaffolds, ACS Appl. Mater. Interfaces 10 (49) (2018) 42933–42940.
- [21] C.M. Portela, A. Vidyasagar, S. Krödel, T. Weissenbach, D.W. Yee, J.R. Greer, D.M. Kochmann, Extreme mechanical resilience of self-assembled nanolabyrinthine materials, Proc. Natl. Acad. Sci. 117 (11) (2020) 5686–5693.
- [22] J. Bauer, L.R. Meza, T.A. Schaedler, R. Schwaiger, X. Zheng, L. Valdevit, Nanolattices: an emerging class of mechanical metamaterials, Adv. Mater. 29 (40) (2017) 1701850.
- [23] G. Oliveri, J.T. Overvelde, Inverse design of mechanical metamaterials that undergo buckling, Adv. Funct. Mater. 30 (12) (2020) 1909033.
- [24] Z. Vangelatos, G.X. Gu, C.P. Grigoropoulos, Architected metamaterials with tailored 3D buckling mechanisms at the microscale, Extreme Mech. Lett. 33 (2019) 100580.
- [25] Y. Jiang, Q. Wang, Highly-stretchable 3D-architected mechanical metamaterials, Sci. Rep. 6 (1) (2016) 1–11.
- [26] M. Spagnuolo, M.E. Yildizdag, U. Andreaus, A.M. Cazzani, Are higher-gradient models also capable of predicting mechanical behavior in the case of wide-knit pantographic structures? Math. Mech. Solids 26 (1) (2021) 18–29
- [27] M. Jamshidian, N. Boddeti, D.W. Rosen, O. Weeger, Multiscale modelling of soft lattice metamaterials: Micromechanical nonlinear buckling analysis, experimental verification, and macroscale constitutive behaviour, Int. J. Mech. Sci. 188 (2020) 105956.
- [28] S. Yin, W. Guo, H. Wang, Y. Huang, R. Yang, Z. Hu, D. Chen, J. Xu, R.O. Ritchie, Strong and tough bioinspired additive-manufactured dual-phase mechanical metamaterial composites, J. Mech. Phys. Solids 149 (2021) 104341.
- [29] M.-S. Pham, C. Liu, I. Todd, J. Lertthanasarn, Damage-tolerant architected materials inspired by crystal microstructure, Nature 565 (7739) (2019) 305–311.
- [30] L. Mizzi, D. Attard, R. Gatt, P.-S. Farrugia, J.N. Grima, An analytical and finite element study on the mechanical properties of irregular hexachiral honeycombs, Smart Mater. Struct. 27 (10) (2018) 105016.
- [31] W.P. Moestopo, A.J. Mateos, R.M. Fuller, J.R. Greer, C.M. Portela, Pushing and pulling on ropes: hierarchical woven materials, Adv. Sci. 7 (20) (2020) 2001271.
- [32] J.J. Andrew, P. Verma, S. Kumar, Impact behavior of nanoengineered, 3D printed plate-lattices, Mater. Des. 202 (2021) 109516.
- [33] C. Broeckhoven, A. du Plessis, C. Hui, Functional trade-off between strength and thermal capacity of dermal armor: insights from girdled lizards, J. Mech. Behav. Biomed. Mater. 74 (2017) 189–194.
- [34] W. Huang, D. Restrepo, J.-Y. Jung, F.Y. Su, Z. Liu, R.O. Ritchie, J. McKittrick, P. Zavattieri, D. Kisailus, Multiscale toughening mechanisms in biological materials and bioinspired designs, Adv. Mater. 31 (43) (2019) 1901561.
- [35] D. Sen, M.J. Buehler, Structural hierarchies define toughness and defecttolerance despite simple and mechanically inferior brittle building blocks, Sci. Rep. 1 (1) (2011) 1–9.
- [36] A. Woesz, J.C. Weaver, M. Kazanci, Y. Dauphin, J. Aizenberg, D.E. Morse, P. Fratzl, Micromechanical properties of biological silica in skeletons of deep-sea sponges, J. Mater. Res. 21 (8) (2006) 2068–2078.
- [37] A. Zampieri, G.T. Mabande, T. Selvam, W. Schwieger, A. Rudolph, R. Hermann, H. Sieber, P. Greil, Biotemplating of luffa cylindrica sponges to self-supporting hierarchical zeolite macrostructures for bio-inspired structured catalytic reactors, Mater. Sci. Eng. C 26 (1) (2006) 130–135.
- [38] H. Ehrlich, E. Brunner, P. Simon, V.V. Bazhenov, J.P. Botting, K.R. Tabachnick, A. Springer, K. Kummer, D.V. Vyalikh, S.L. Molodtsov, et al., Calcite reinforced silica-silica joints in the biocomposite skeleton of deep-sea glass sponges, Adv. Funct. Mater. 21 (18) (2011) 3473–3481.
- [39] M.A. Monn, J.C. Weaver, T. Zhang, J. Aizenberg, H. Kesari, New functional insights into the internal architecture of the laminated anchor spicules of Euplectella aspergillum, Proc. Natl. Acad. Sci. 112 (16) (2015) 4976–4981.

- [40] W.E. Müller, X. Wang, B. Sinha, M. Wiens, H.-C. Schröder, K.P. Jochum, Nanosims: insights into the organization of the proteinaceous scaffold within hexactinellid sponge spicules, ChemBioChem 11 (8) (2010) 1077–1082.
- [41] W.E. Müller, X. Wang, K. Kropf, H. Ushijima, W. Geurtsen, C. Eckert, M.N. Tahir, W. Tremel, A. Boreiko, U. Schloß macher, et al., Bioorganic/inorganic hybrid composition of sponge spicules: matrix of the giant spicules and of the comitalia of the deep sea hexactinellid monorhaphis, J. Struct. Biol. 161 (2) (2008) 188–203.
- [42] H. Le Ferrand, External fields for the fabrication of highly mineralized hierarchical architectures, J. Mater. Res. 34 (1) (2019) 169–193.
- [43] X. Wang, H.C. Schroeder, K. Wang, J.A. Kaandorp, W.E. Mueller, Genetic, biological and structural hierarchies during sponge spicule formation: From soft sol-gels to solid 3D silica composite structures, Soft Matter 8 (37) (2012) 9501–9518.
- [44] J. Aizenberg, J.C. Weaver, M.S. Thanawala, V.C. Sundar, D.E. Morse, P. Fratzl, Skeleton of euplectella sp.: structural hierarchy from the nanoscale to the macroscale, Science 309 (5732) (2005) 275–278.
- [45] J.C. Weaver, J. Aizenberg, G.E. Fantner, D. Kisailus, A. Woesz, P. Allen, K. Fields, M.J. Porter, F.W. Zok, P.K. Hansma, et al., Hierarchical assembly of the siliceous skeletal lattice of the hexactinellid sponge Euplectella aspergillum, J. Struct. Biol. 158 (1) (2007) 93–106.
- [46] S. Morankar, A.S.S. Singaravelu, S. Niverty, Y. Mistry, C.A. Penick, D. Bhate, N. Chawla, Tensile and fracture behavior of silica fibers from the venus flower basket (Euplectella aspergillum), Int. J. Solids Struct. (2022) 111622.
- [47] M.C. Fernandes, J. Aizenberg, J.C. Weaver, K. Bertoldi, Mechanically robust lattices inspired by deep-sea glass sponges, Nature Mater. 20 (2) (2021) 237–241.
- [48] G. Falcucci, G. Amati, P. Fanelli, V.K. Krastev, G. Polverino, M. Porfiri, S. Succi, Extreme flow simulations reveal skeletal adaptations of deep-sea sponges, Nature 595 (7868) (2021) 537–541.
- [49] A. Miserez, J.C. Weaver, P.J. Thurner, J. Aizenberg, Y. Dauphin, P. Fratzl, D.E. Morse, F.W. Zok, Effects of laminate architecture on fracture resistance of sponge biosilica: Lessons from nature, Adv. Funct. Mater. 18 (8) (2008) 1241–1248.
- [50] S.M. Esfarjani, A. Dadashi, M. Azadi, Topology optimization of additive-manufactured metamaterial structures: A review focused on multi-material types, Forces Mech. (2022) 100100.
- [51] O.M. Querin, M. Victoria, P. Martí, Topology optimization of truss-like continua with different material properties in tension and compression, Struct. Multidiscip. Optim. 42 (1) (2010) 25–32.
- [52] M. Spagnuolo, M.E. Yildizdag, X. Pinelli, A. Cazzani, F. Hild, Out-of-plane deformation reduction via inelastic hinges in fibrous metamaterials and simplified damage approach, Math. Mech. Solids 27 (6) (2022) 1011–1031.
- [53] F. dell'Isola, I. Giorgio, M. Pawlikowski, N.L. Rizzi, Large deformations of planar extensible beams and pantographic lattices: heuristic homogenization, experimental and numerical examples of equilibrium, Proc. R. Soc. A: Math. Phys. Eng. Sci. 472 (2185) (2016) 20150790.
- [54] D. Chen, X. Zheng, Multi-material additive manufacturing of metamaterials with giant, tailorable negative Poisson's ratios, Sci. Rep. 8 (1) (2018) 1-8.
- [55] C. Lin, L. Zhang, Y. Liu, L. Liu, J. Leng, 4D printing of personalized shape memory polymer vascular stents with negative Poisson's ratio structure: A preliminary study, Sci. China Technol. Sci. 63 (4) (2020) 578–588.
- [56] S. Yin, Z. Jia, X. Li, J. Zhu, Y. Xu, T. Li, Machine-learning-accelerated design of functional structural components in deep-sea soft robots, Extreme Mech. Lett. 52 (2022) 101635.
- [57] L. Liew, W. Zhang, L. An, S. Shah, R. Luo, Y. Liu, T. Cross, M.L. Dunn, V. Bright, J.W. Daily, et al., Ceramic MEMS, Am. Ceram. Soc. Bull. 80 (5) (2000) 25
- [58] V. Srikar, S.D. Senturia, The reliability of microelectromechanical systems (MEMS) in shock environments, J. Microelectromech. Syst. 11 (3) (2002) 206–214.
- [59] W. Hao, D. Ge, Y. Ma, X. Yao, Y. Shi, Experimental investigation on deformation and strength of carbon/epoxy laminated curved beams, Polym. Test. 31 (4) (2012) 520–526.
- [60] P. Talebizadehsardari, A. Eyvazian, M. Asmael, B. Karami, D. Shahsavari, R.B. Mahani, Static bending analysis of functionally graded polymer composite curved beams reinforced with carbon nanotubes, Thin-Walled Struct. 157 (2020) 107139.